A critical local energy release rate criterion for fatigue fracture of elastomers

Samy Mzabi, Daniel Berghezan, Stéphane Roux, François Hild, Costantino Creton

A Critical Local Energy Release Rate Criterion for Fatigue Fracture of Elastomers

Samy Mzabi,[1]* Daniel Berghezan,[2] Stéphane Roux,[3] Francois Hild,[3] Costantino Creton[1]

[1]Laboratoire PPMD, ESPCI-PARISTECH, 10 Rue Vauquelin, 75231 Paris Cedex 05, France

[2]Michelin, Centre Technique de Ladoux, Clermont-Ferrand, France

[3]LMT-Cachan, ENS de Cachan, CNRS, Université Paris 6, PRES UniverSud Paris, 61 Avenue du Président Wilson, F-94235 Cachan Cedex, France

Correspondence to: C. Creton (E-mail: costantino.creton@espci.fr)

Received 22 May 2011; revised 13 July 2011; accepted 13 July 2011; published online 7 September 2011
DOI: 10.1002/polb.22338

ABSTRACT: Using Digital Image Correlation on high-resolution images, the full strain field near the tip of a crack propagating under cyclic loading in an elastomer was characterized. We show unambiguously, and for the first time, the existence of a strongly localized and highly oriented process zone close to the crack tip and propose a simple physical model introducing a local energy release rate $g_{local} = W_{unloading}H_0$, where $W_{unloading}$ is the unloading strain energy density in uniaxial tension at the maximum strain measured at the crack tip, and H_0 is the undeformed size of the highly stretched zone in the loading direction. Remarkably, the crack growth rate under cyclic loading is found to fall on a master curve as a function of g_{local} for three elastomers with different filler contents and crosslinking densities, while the same crack growth rate as a function of the applied macroscopic energy release rate G, differs by two orders of magnitude for the same three elastomers.

INTRODUCTION Because of their remarkable behavior, elastomers are used nowadays in a large variety of applications as structural but flexible materials. In many of those engineering applications, failure of the component occurs by the propagation of a crack. Therefore, studying crack propagation is a usual way to test both tear resistance (for single loading failure) and fatigue resistance (under cyclic loading). Significant efforts have been made by both the physics and the mechanics community to develop models relating the linear viscoelastic properties of the rubber to its fracture behavior.[1–5] Although these theories have been qualitatively successful, they cannot predict quantitatively the fracture energy because they ignore the large strain region near the crack tip.[6] This shortcoming is even more pronounced when it comes to crack propagation under cyclic loading where stresses and strains are relatively low in most of the material and most of the dissipated energy simply heats the sample without causing any damage. Typically, the fatigue resistance is characterized by carrying out experiments of cyclic tensile loading on notched samples with the so-called "pure shear geometry."[7] Below a certain threshold G_0 in applied energy release rate G, the crack does not grow at all in the absence of a chemical attack. Then a regime is observed where:

$$\frac{dc}{dN} = \beta(G - G_0) \quad (1)$$

where c is the crack length, N is the number of cycles, and β is a material dependent constant. As the applied G increases, the propagation rate enters in a logarithmic regime where:

$$\frac{dc}{dN} = AG^{\alpha} + B \quad (2)$$

where A, B, and α are material-dependent constants. Finally, above a critical value G_c, catastrophic propagation is observed. The prediction of the crack propagation velocity per cycle in a fatigue experiment from simple viscoelastic material properties and loading conditions is currently highly empirical,[8] and there is no available physically based model bridging the length scales from molecular fracture to macroscopic loading conditions as it exists, say, for glassy polymers.[9–11] The first step in developing such a model is a better characterization of the strain field in the vicinity of the crack tip. Elastomers have a low elastic modulus, and strains can be very large before fracture over a reasonably large volume, making real-time optical techniques very attractive.

**Present address:* Goodyear Innovation Center Luxembourg, Avenue Gordon Smith, L-7750 Colmar-Berg, Luxembourg.

TABLE 1 Composition (in weight) and Main Physical Characteristics of the Filled Polymers Used. Volume Fraction of Filler ϕ and Crosslink Density ν

	3CB_8XL	20CB_8XL	20CB_15XL
SBR	100	100	100
N347	5	50	50
6PPD	1	1	1
Struktol	3	3	3
CBS	1.5	1.5	1.5
Sulfur	1.5	1.5	2.5
ϕ	0.03	0.2	0.2
ν (mol/cm^3)[a]	8.1×10^{-5}	7.1×10^{-5}	18.9×10^{-5}

[a] Determined from swelling experiments by Michelin.

Many experimental techniques have been used to study the strain field close to a crack tip such as speckle interferometry,[12] moiré interferometry,[13] the grid method,[14] and photoelasticity.[14,15] However, those techniques can hardly be used at different length scales with nontransparent materials. The experimental technique used in this study is Digital Image Correlation (DIC). This method for measuring full displacement fields has known important improvements in accuracy and availability during those last 30 years, thanks to the development of better algorithms, computers and electronics and is well suited for the measurements of displacement fields from various types of images. The DIC tool that we used, CORRELI[Q4], uses a random texture at the surface of the studied sample (i.e., random distribution of markers that induces heterogeneous gray levels). The difference in the image of the random texture before and during deformation of the material is used to reconstruct the displacement field. With a proper algorithm, centipixel resolutions are achieved.[16]

MATERIALS AND METHODS

We investigated the fatigue fracture of three different noncrystallizing elastomers, based on the same styrene-butadiene random copolymer (SBR) filled with carbon black (reference N347) but with different filler contents and different levels of sulfur-based crosslinking. The SBR has a M_n of 120 kg/mol and a polydispersity of 1.94. Its styrene content is 15 wt % and the T_g measured by differential scanning calorimetry (DSC) is -48 °C.

The composition of the selected filled polymers before vulcanization is presented in Table 1. Vulcanization is carried out with sulfur; 2-cyclohexylbenzothiazole-2-sulfenamide (CBS) and STRUKTOL ZEH are used as accelerators; *N*-(1,3-dimethylbutyl)-*N*′-phenyl-*p*-phenylenediamine (6PPD) is used as an antioxidant.

All samples were prepared, molded, and cured by Michelin. The crosslink density was obtained by swelling experiments taking into account that the filler is not swellable and assuming that the presence of the filler does not alter vulcanization. For tensile tests, the samples were dog-bone shape with a cross-section of 2 × 4 mm. For the crack propagation experiments, the samples were "pure shear" geometries, that is, strips of length $l_0 = 157$ mm, height $h_0 = 13$ mm, and thickness $t_0 = 2$ mm. Two edge cracks and a center crack were cut with a razor blade in the direction parallel to the length as commonly done for fatigue crack propagation experiments. When tensile loading cycles (from $\varepsilon = 0$ to $\varepsilon = \varepsilon_{PS}$) are applied to such precracked samples, the shape of the crack tip and the crack propagation rate per cycle goes through a transient that is poorly reproducible. After typically 5000 cycles, the system evolves toward a steady state where the crack propagation velocity and crack tip shape remain nearly constant. We only considered measurements in the latter steady-state regime.

A key parameter driving crack propagation in these cyclic tests is the maximum energy release rate G applied to the crack that depends on the strain applied to pure-shear samples ε_{PS}. It is simply given by[17]:

$$G = W_{PS}(\varepsilon_{PS})h_0 \tag{3}$$

where $W_{PS}(\varepsilon_{PS})$ is the strain energy density as a function of applied strain in the pure shear geometry. $W_{PS}(\varepsilon_{PS})$ is conventionally defined from the integral under the loading curve from $\varepsilon = 0$ to $\varepsilon = \varepsilon_{PS}$ of identical but uncracked samples that have been previously strained 1000 times to a value of ε_{PS} larger than that applied during the fatigue tests (to avoid the so-called Mullins effect). In our case, the samples were preconditioned in this way at $\varepsilon_{PS} = 27\%$.

The preconditioned samples were then notched and cycled for about 50,000 cycles at a value of G corresponding to $\varepsilon_{PS} = 23\%$. In this geometry, the applied G does not depend on the crack length c. However, during the first few thousand cycles, the crack propagation rate and the crack radius evolve. We only measured crack tip strain fields once the field was stationary. Measurements of the crack tip strain field were made for G varying between 500 and 3000 J/m^2 which typically implies values of ε_{PS} varying between 5 and 23%.

The displacement and strain fields near the crack tip were determined by DIC using four-noded (Q4) elements discretizing the region of interest.[16] Images were taken with a CANON EOS 40D camera (resolution of 10.1 Megapixels) fixed on a tripod, with a macro-objective 100/2.8 with extension rings or with a binocular objective (in which case the pixel size reached ~1.6 μm). The size of the region of interest was 6.5 × 4.5 mm^2. Light was provided by a cold source (Schott, model KL 1500 LCD) with a power of 150 W fitted with semirigid optical fibers to adjust and focus the light beam. The random texture was provided by talcum powder that once sprinkled, showed the best distribution in terms of gray levels. Furthermore, the size of the particles is small, (ca. 10 μm) and the talcum powder has a good adhesion with rubber (e.g., electrostatic, and Van der Waals interactions). Once the images are acquired and treated, the image correlation tool decomposes the global displacement $\boldsymbol{u}$ according to its vertical and horizontal component (u_1 and u_2, respectively).

In order to measure the displacement field of a deformed configuration from a reference one, the images were meshed with a regular square grid with elements of size 26 μm (or 16 pixels). The image correlation procedure consists in

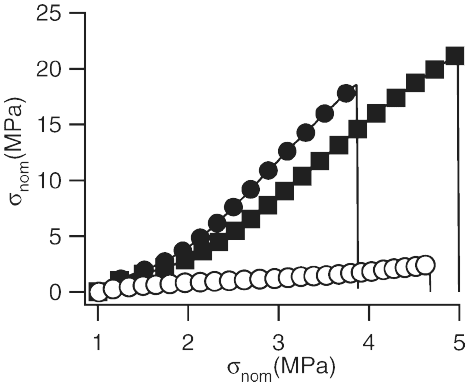

FIGURE 1 Stress–strain curves in uniaxial extension until fracture. ■: 20CB_8XL; ○: 3CB_8XL; ●: 20CB_15XL.

determining the displacement field decomposed over bilinear shape functions over the elements between two images taken at different moments. The uncertainty of the method is in the range of 2/100 pixel, and the resolution is about 1/100 pixel. For a uniform strain field, it has been found that the standard uncertainty was of the order of 10^{-4}. Its advantages are: (i) a fast procedure, (ii) the spatial resolution does not depend on the configuration of the correlation algorithm, (iii) the preparation of the surface is not always necessary, (iv) the interpolation algorithm permits to reach subpixel resolutions, and (v) it requires only a light equipment (digital camera + macro-objective or binocular). However, the image acquisition conditions have to be carefully controlled: (i) the creation of a random texture, (ii) the alignment of the camera with the sample, and (iii) the lighting system.

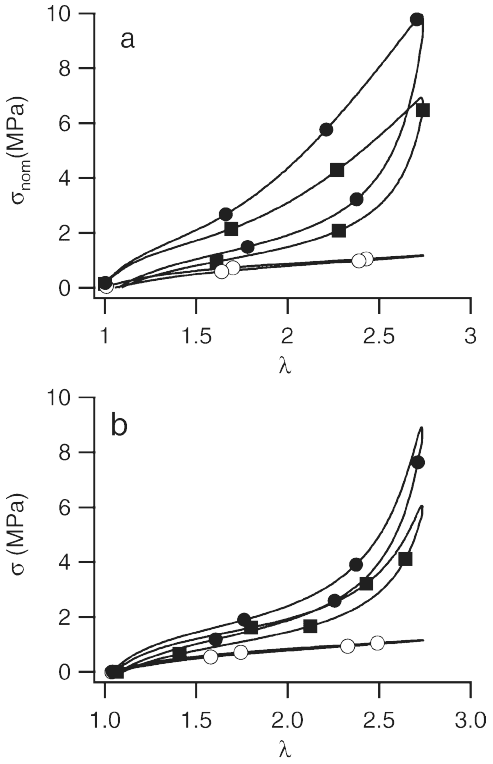

FIGURE 2 Hysteresis cycles in uniaxial extension for the three materials. (a) first cycle and (b) second cycle. ■: 20CB_8XL; ○: 3CB_8XL; ●: 20CB_15XL.

RESULTS

Tensile Tests and Hysteresis Tests

In order to characterize the material properties which will be needed to interpret the fracture data, we report on Figure 1 the stress–strain curves of the three materials in uniaxial extension until fracture and in Figure 2 the hysteresis observed in uniaxial extension for the first cycle (so-called Mullins hysteresis) and for the second cycle.

As reported by many, the presence of fillers stiffens significantly the polymer and creates a large hysteresis loop during the first cycle and a much smaller one for the second (and subsequent) cycles. The detailed physical interpretation of the hysteresis of the first cycle is a matter of debate to this day[18] but is due to a modification of the structure of the filled elastomer. The change in crosslinking from 20CB_8XL to 20CB_15XL_ has an effect on the stiffness and on the hysteresis of the first cycle but not much on the hysteresis of the subsequent cycles.

Fatigue Experiments

Figure 3 shows the measured crack growth rates per cycle in the steady state regime as a function of the applied G. dc/dN for the three elastomers increase with G^n as reported in the literature for a variety of elastomer systems.[8] It is however clear from the data that the three elastomers present orders of magnitude differences in terms of crack growth rate for the same applied G. The sample with the lowest filler content has the highest crack propagation rate while the degree of crosslinking has a major influence on crack propagation for the two filled samples.

The difference between 3CB_8XL and 20CB_8XL materials can be qualitatively explained by a difference in dissipative properties. However, as shown in Table 2, the energy dissipated per cycle in the second cycle at $\varepsilon = 175\%$ is not very

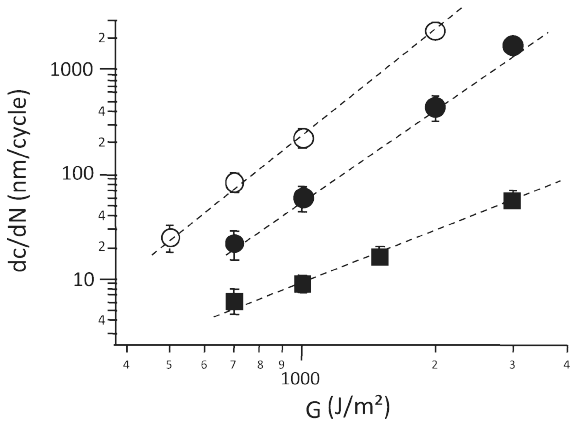

FIGURE 3 Crack growth rate per cycle in the steady-state regime as a function of applied macroscopic G. ■: 20CB_8XL; ○: 3CB_8XL; ●: 20CB_15XL.

TABLE 2 Hysteresis During Loading–Unloading Cycles at ε = 175% for the Three Studied Elastomers

Blend	3CB_8XL	20CB_8XL	20CB_15XL
W_{second_cycle} (MJ/m^3)	0.16	0.84	0.99
$W_{Mullins}$ (MJ/m^3)	0.22	2.52	3.63

different. At identical strain levels, 20CB_15XL is more dissipative than 20CB_8XL, and yet, the crack propagates significantly faster in 20CB_15XL. Therefore, the conventional wisdom equating higher dissipation with slower crack growth rate[19] would not explain the present data.

Strain Field Measured by DIC

Figure 4(a) is an example of displacement field (the color bar is in pixels) obtained in the case of a prenotched rubber sample to which we applied a far-field strain of $\varepsilon_{PS} = 23\%$ (1 pixel $\leftrightarrow$ 1.6 μm). The data was collected statically but after a few thousand cycles were applied to the samples at the same value of $\varepsilon_{PS} = 23\%$.

In Figure 4(a), the shape of the contours shows distinctively the presence of a singularity. Far from the crack tip, the contours are quasi-parallel to the horizontal axis denoting a uniform strain. The direction normal to the applied force shows some displacement but much smaller than along the direction parallel to it and in the following analysis it will be neglected. Our primary interest is to characterize the strain fields close to the crack tip to obtain some physical insights. We focused on the values of u_1 in the x_1 direction at different distances from the crack tip as shown schematically in Figure 4(a). Far from the crack tip (line a), u_1 is a straight line with a slope corresponding to the uniform far field strain applied to the remainder of the sample (in this example 23%). Closer to the crack tip (line c), the displacement shows a change in slope, and the strain at the level of the crack axis exceeds 100%. The change of slope between line *a* and line *c* shows that there is a transition between the pure shear state and a zone of influence near the crack where the strain levels are significantly higher. We define here ε_{11} in each point along the x_1 direction by taking du_1/dx_1 for each point of interest. The maximum value of ε_{11} (at $x_1 = 0$) as a function of the distance x_2 ahead of the crack tip, shown in Figure 5, allows us to distinguish:

- The pure shear zone is the region where the measured strain is on average equal to the applied far-field strain, $\varepsilon_{PS} = 23\%$ in the previous example.
- The zone of influence (L_{ZI}) is the area where the singularity has an effect on the strain field ($\sim$2 mm in the example of Fig. 5).

The interesting result is that the local strain values at the crack tip are markedly different for the three elastomers for the same value of ε_{PS} as shown in Figure 6. The lower filler content sample 3CB_8XL has a very high value of ε_{11} at the crack tip while the two filled systems have much lower values. This implies significant differences in the full strain fields near the crack tip due to nonlinear mechanical material properties. In either case, this difference is very reproducible and cannot be attributed to differences in initial state.

Because of the discretization and of the resolution of our mesh we cannot determine the value of ε_{11} precisely at the crack tip. However, we can extrapolate linearly between the

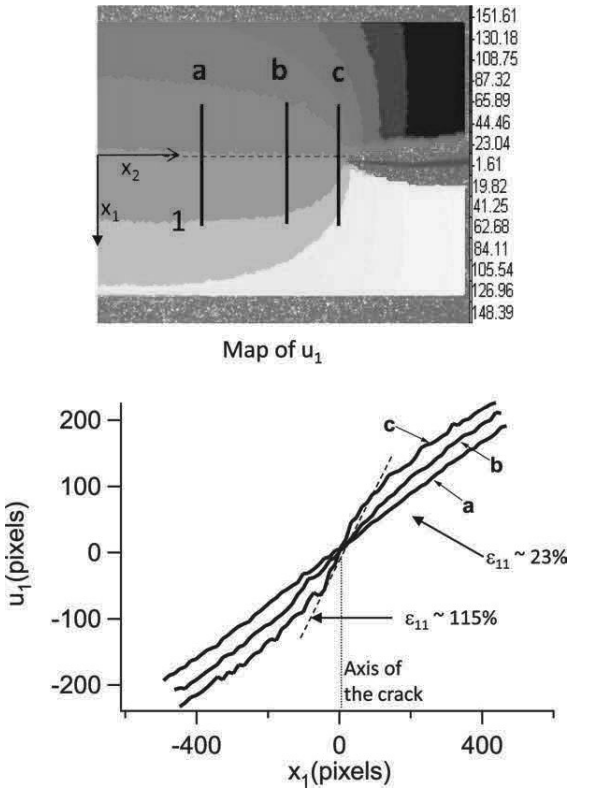

FIGURE 4 (a) Displacement field u_1 obtained by DIC as a function of position x_1 (vertical) and x_2 (horizontal) in the undeformed configuration of a propagating crack. The far-field strain is here $\varepsilon = 23\%$. (b) Displacement u_1 as a function of the distance along the x_1 direction (perpendicular to the crack propagation direction) for the three material lines shown in Figure 4(a). 1 pixel = 1.6 μm

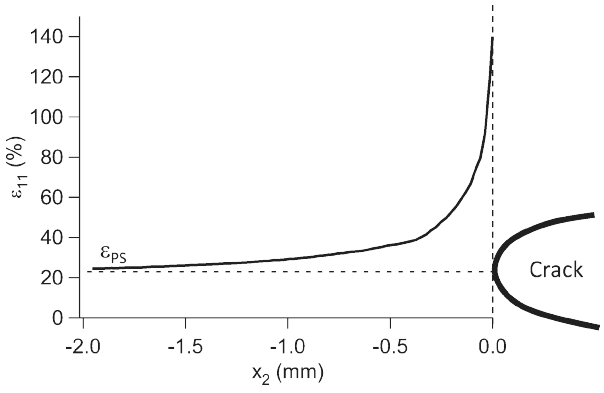

FIGURE 5 Strain ε_{11} as a function of x_2 for the 20CB_8XL material at $\varepsilon_{PS} = 23\%$. The crack tip is located at $x_2 = 0$.

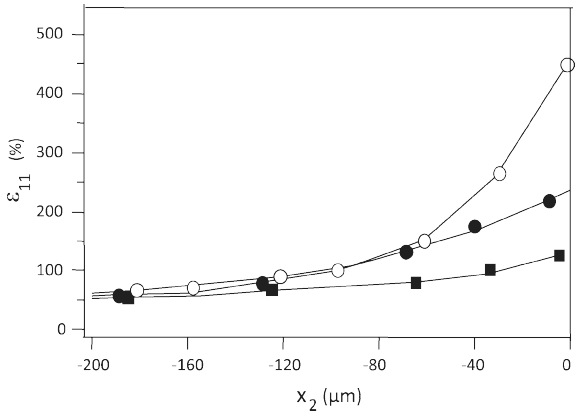

FIGURE 6 ε_{11} as a function of position along x_2 direction for the three elastomers. The crack tip is located at $x_2 = 0$. ■: 20CB_8XL; ○: 3CB_8XL; ●: 20CB_15XL.

last measurable value of ε_{11} and the crack tip. We used this approximation to define a value for ε_{max} for each material and for each value of applied ε_{PS}. Figure 7 shows the measured values of ε_{max} as a function of ε_{PS} for the three elastomers and highlights the key difference in behavior. The 3CB_8XL material is highly stretched at the crack tip since the absence of fillers reduces the ability of the material to smooth strain concentrations at the crack tip. The presence of a network of fillers adding stiffness at low strains favors this creep process (see 20CB_8XL grade) but an excessive crosslinking hinders significantly this local creep mechanism.

A Simple Model

Figures 4 and 5 show that a highly strained zone exists at the crack tip where the strain decreases weakly with position along the x_1 direction away from the crack axis and very sharply along the x_2 direction. This is typical of hyperelastic large strain fields.[20] We propose to model this highly strained zone approximately as a homogeneously strained zone (at constant strain ε_{max}) of undeformed height H_0 [determined by selecting the range of values of x_i where $\varepsilon_{11} > 0.9\ \varepsilon_{max}$. This zone is approximately equivalent to the region delimited by the inflexion points in line c of Fig. 4(b)]. A value of H_0 and ε_{max} can then be determined for each material and each value of ε_{PS} with the procedure outlined above.

The existence of such a highly strained zone near the crack tip can be compared with what occurs in glassy polymers when craze fibrils form.[21] Brown has proposed a successful model to predict the fracture toughness of such polymer glasses from the observation of the structure of the highly stretched craze.[9] He introduced a local energy release rate g_{local} as the product of the elastic strain energy density in the stretched zone (assuming this zone is fully elastic) by the width of the stretched craze. When g_{local} exceeds a critical value, fracture of the craze occurs. The interesting feature of that model is that it focuses on determining a credible molecular fracture criterion rather than a precise evaluation of where the energy is dissipated. It assumes that the elastic energy in the region outside of the craze is not available for fracture but is screened by the dissipative zone where the polymer chains are being plastically oriented, that is, at the interface between the isotropic zone and the oriented zone. In our case, the localization of the oriented zone is much less marked but nevertheless a stretching zone above and below the crack propagation axis exists right in front of the crack tip as shown by the inflection points of Figure 4. Adapting Brown's insight to our rubbers, we assume that the highly stretched zone at the crack tip can be a nonlinear elastic zone which releases deformation (or elastic) energy when the crack propagates.

We define an approximate local energy release rate as:

$$g_{local} = W_{unloading} H_0 \tag{4}$$

where $W_{unloading}$ is given by:

$$W_{unloading} = \int_0^{\varepsilon_{max}} \sigma d\varepsilon \tag{5}$$

under the first unloading curve. $W_{unloading}$ can be calculated for each value of ε_{max} reported in Figure 5 and is the best estimate we have of the density of elastic energy in the highly stretched zone.

The local g defined in eq 4 assumes that only the energy stored in the highly oriented zone close to the crack tip is available to break the bonds. This is a bold assumption but it can be justified (arguably) by the shape of the deformation field in the x_1 direction. The presence of two zones [at the inflection points in Fig. 2(b)] where the strain in the x_1 direction changes significantly over a small distance and where the polymer is being stretched screens the elastic energy coming from outside the stretched zone. The simplified physical picture of the crack tip zone is shown on Figure 8.

The validity of this assumption is however mostly supported by the results of the crack propagation experiments. Figure 9 shows the values of dc/dN of Figure 3 as a function of g_{local} as defined in eq 4. Remarkably, the rate of crack growth now

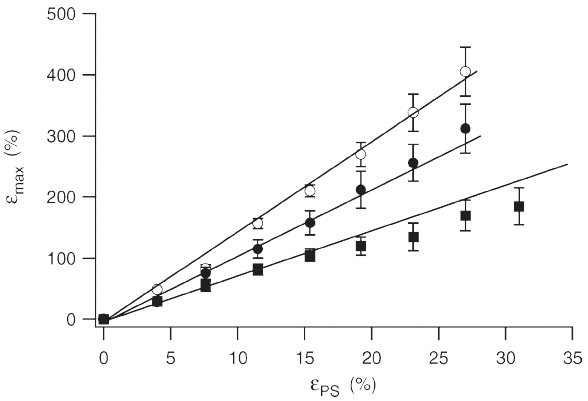

FIGURE 7 Values of ε_{max} as a function of ε_{PS}. ■: 20CB_8XL; ○: 3CB_8XL; ●: 20CB_15XL.

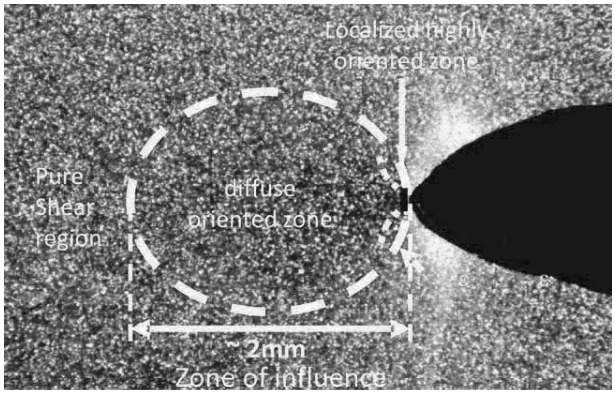

FIGURE 8 Scheme of the deformation zones ahead of the crack tip.

appears to be a unique function of g_{local}. Within that range of applied macroscopic G, the dependence of dc/dN with g_{local} can be represented by the empirical expression:

$$\frac{dc}{dN} = \left(\frac{dc}{dN}\right)_0 \left(1 + \left(\frac{g_{local}}{g*}\right)^n\right) \quad (6)$$

with $(dc/dN)_0 \sim 4$ nm/cycle, $g^* \sim 60$ J/m^2, and $n \sim 1.8$. This universal scaling behavior suggests that the failure criterion depends solely on g_{local} rather than on G and that there are two distinct regimes, a threshold where dc/dN does not depend much on g_{local} and a power-law regime.

In other words, the toughness of the rubber depends on its ability to form a highly stretched zone at the crack tip. An unfilled rubber is able to form such a highly stretched zone with a relatively low applied macroscopic G, while the toughest rubbers require a much higher applied G value to obtain the same level of stretching, or more exactly the same level of stored elastic energy in the highly stretched zone.

The question of the regime of validity of the model should now be discussed. The set of parameters g^*, $(dc/dN)_0$ and n of eq 3 is probably characteristic of the specific base polymer used, and of the crosslinking chemistry but only applies to the logarithmic regime of crack propagation (eq 2) where g_{local} can be clearly defined. At lower G, dc/dN varies linearly with applied G (eq 1), the highly stretched zone of Figure 8 is not detectable and g_{local} is difficult to define. This is analogous to the threshold observed for the onset of crazing in glassy polymers and corresponds to the onset of significant polymer "orientation."[11] Therefore, there must be a threshold in G and in ε_{PS} below which the model does not apply and the physical meaning of g^*, remains unclear at the moment. Only new strain field measurements in this low G regime could shed some light on how fracture occurs in fatigue at that low level of G.

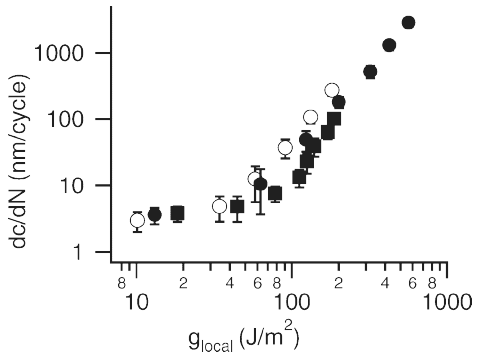

FIGURE 9 Crack growth rate as a function of the local energy release rate for the three studied elastomers. ■: 20CB_8XL; ○: 3CB_8XL; ●: 20CB_15XL.

DISCUSSION

Although the model is admittedly simple, it captures the key features of the differences between elastomers having various filler contents and crosslinking densities for crack propagation in fatigue. The key factor controlling resistance to crack growth is the capacity of the material to reduce (or average) elastic energy density in a local zone close to the crack tip for the same applied global energy release rate. This reduction in the level of stored elastic energy close to the crack tip makes bond-breaking less probable for each cycle. It appears to be most effective for highly filled but not very crosslinked elastomers. This is illustrated in Figure 10 showing the measured values of g_{local} as a function of the applied macroscopic G for the three elastomers.

It is well known that a minimum amount of filler is necessary in the elastomer to display the characteristic increase in modulus at small strain, softening at intermediate strains and increase in fracture toughness.[22] This minimum amount of filler is believed to create a "damageable" filler network where fillers can rearrange under stress[18] and soften the elastomer when stretched. An excessive crosslinking probably prevents such rearrangement. The probability of failure of a chemical bond under repeated loads appears to be controlled by the available strain energy in the immediate vicinity of the crack tip so that tough materials are those where a very large difference exists between g_{local} and G for the same

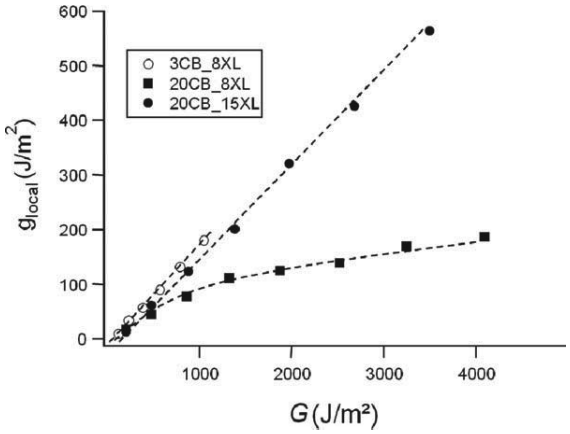

FIGURE 10 g_{local} as a function of G for the three studied elastomers. ■: 20CB_8XL; ○: 3CB_8XL; ●: 20CB_15XL.

applied strain ε_{PS}. Furthermore, the level of viscoelastic dissipation (measured by the hysteresis of a stabilized cycle) or of dissipation due to Mullins' effect (measured by the hysteresis of the first cycle), can partly explain the filler effect but cannot explain even qualitatively the effect of changing the crosslink density. Unfortunately, more detailed comparisons with a model based on using the full-linear viscoelastic spectrum to predict crack propagation[19] are difficult to make for filled elastomers because viscoelastic dissipation in filled elastomers depends markedly on strain history (which depends on position near the crack tip).

A discussion could not be complete without some critical assessment. A key question in fracture problems is always where the energy is dissipated. Our hypothesis is that there is a highly stretched and relatively localized region near the crack tip where energy dissipation is low and mostly due to bond breakage, which is surrounded by a highly dissipative zone where the polymer chains are being stretched and the spatial arrangement of the fillers (if present) is being reorganized. This zone is almost "plastic" in nature. Finally, further away from the crack tip, energy is dissipated simply by classic viscoelasticity mechanisms which are accounted for in.[19] Such a hypothesis is reasonable and consistent with the experimental data reported herein. However, the former is still far from proven in particular in view of the spatial resolution of the strain field data obtained, which precludes the access to the region very close to the crack tip (i.e. less than 15 μm) where most of the damage in the material leading to fracture is likely to take place. However, although the reported experimental estimate of the local energy release rate cannot be considered as an intrinsic quantity (a higher magnification may yield different values), the remarkable coincidence of the crack growth rates with respect to g_{local} (Fig. 9) for all the investigated materials (at the same scale) is striking.

CONCLUSIONS

Using DIC on high-resolution images, we demonstrated the existence of a strongly localized oriented zone close to the crack tip where strains depend markedly on material properties for identical values of far-field strains ε_{PS}. We model this highly stretched zone by a localized and homogeneously strained zone (defined by $\varepsilon_{\max}$ at the crack tip and vertical extension of the process zone H_0) and introduce for the first time for elastomers a local release rate energy $g_{\text{local}} = W_{\text{unloading}} H_0$ that estimates the elastic energy released in the immediate vicinity of the crack tip. The crack growth rate dc/dN versus g_{local} follows a unique behavior for three elastomers with very different crack growth resistance for the same given applied macroscopic G. These results strongly suggest that the eventual fracture of the chemical bonds in the elastomer which trigger crack propagation, is controlled by the elastic energy stored in this oriented zone and that the differences between elastomers in terms of resistance to fracture are dominated by differences in the amount of energy needed to create such a highly stretched zone at the crack tip rather than by differences in intrinsic resistance of the chemical bonds.

ACKNOWLEDGMENTS

The authors thank Fabien Vion-Loisel, Christophe Moriceau, and Maude Portigliatti from Michelin for numerous scientific discussions and for providing all the samples. The authors also gratefully acknowledge Michelin for being the main sponsor of the project and the French ANR (Projet ANR- 08-MAPR-0019) for additional funding.

REFERENCES AND NOTES

1 Mueller, H. K.; Knauss, W. G. *J. Appl. Mech.* **1971,** *38,* 483–488.

2 Schapery, R. A. *Int. J. Fract.* **1975,** *11,* 141–159.

3 Christensen, R. M.; Wu, E. M. *Eng. Fracture. Mech.* **1981,** *14,* 215–225.

4 de Gennes, P. G. *Can. J. Phys.* **1990,** *68,* 1049–1054.

5 Persson, B. N. J.; Albohr, O.; Heinrich, G.; Ueba, H. *J. Phys. Condens. Matter* **2005,** *17,* R1071–R1142.

6 Gent, A. N. *Langmuir* **1996,** *12,* 4492–4496.

7 Lake, G. J. *Rubber Chem. Technol.* **1995,** *68,* 435–460.

8 Mars, W. V.; Fatemi, A. *Rubber Chem. Technol.* **2004,** *77,* 391–412.

9 Brown, H. R. *Macromolecules* **1991,** *24,* 2752–2756.

10 Creton, C., Kramer, E. J.; Brown, H. R.; Hui, C. Y. *Adv Polym. Sci.* **2002,** *156,* 53–136.

11 Sha, Y.; Hui, C. Y.; Ruina, A.; Kramer, E. J. *Macromolecules* **1995,** *28,* 2450–2459.

12 An, W.; Carlsson, T. E. *Opt. Lasers Eng.* **2003,** *40,* 529–541.

13 Morita, Y.; Arakawa, K.; Todo, M. *Opt. Lasers Eng.* **2008,** *46,* 18–26.

14 Andrews, E. H. *Proc. Phys. Soc. London* **1961,** *77,* 483–498.

15 Hui, C. Y.; Jagota, A.; Bennison, S. J.; Londono, J. D. *Proc. R. Soc. London Ser A: Math. Phys. Sci.* **2003,** *403,* 1489–1516.

16 Besnard, G.; Hild, F.; Roux, S. *Exp. Mech.* **2006,** *46,* 789–803.

17 Rivlin, R. S.; Thomas, A. G. *J. Polym. Sci.* **1953,** *10,* 291–318.

18 Diani, J.; Fayolle, B.; Gilormini, P. *Eur. Polym. J.* **2009,** *45,* 601–612.

19 Persson, B. N. J.; Brener, E. A. *Phys. Rev. E.* **2005,** *71,* 036123.

20 Krishnan, V. R.; Hui, C. Y.; Long, R. *Langmuir* **2008,** *24,* 14245–14253.

21 Kramer, E. J.; Berger, L. L. *Adv. Polym. Sci.* **1990,** *91/92,* 1–68.

22 Heinrich, G.; Kluppel, M.; Vilgis, T. A. *Curr. Opin. Solid State Mater. Sci.* **2002,** *6,* 195–203.